Transition metal migration and O_2 formation underpin voltage hysteresis in oxygen-redox disordered rocksalt cathodes

Kit McColl,[1,2] Robert A. House,[2,3] Gregory J. Rees,[2,3] Samuel W. Coles,[1,2] Alexander G. Squires,[1,2] Peter G. Bruce,[2,3,4] Benjamin J. Morgan,[1,2] and M. Saiful Islam[1,2,*]

[1]*Department of Chemistry, University of Bath, Claverton Down, BA2 7AY, UK*
[2]*The Faraday Institute, Quad One, Harwell Science and Innovation Campus, Didcot, OX11 0RA, UK*
[3]*Department of Materials, University of Oxford, Oxford, OX2 6NN, UK*
[4]*Department of Chemistry, University of Oxford, Oxford, OX1 3TA, UK*

Lithium-rich disordered rocksalt cathodes display high capacities arising from redox chemistry on both transition-metal and oxygen ions and are potential candidates for next-generation lithium-ion batteries. The atomic-scale mechanisms governing this O-redox behaviour, however, are not fully understood. In particular, it is not clear to what extent transition metal migration is required for O-redox and what role this may play in explaining voltage hysteresis in these materials. Here, we reveal an O-redox mechanism linking transition metal migration and O_2 formation in the disordered rocksalt Li_2MnO_2F. At high states of charge, O-ions dimerise to form molecular O_2 trapped in the bulk structure, leaving vacant O sites surrounding neighbouring Mn ions. This undercoordination drives Mn movement into new fully-coordinated octahedral sites. Mn displacement can occur irreversibly, which results in voltage hysteresis, with a lower voltage upon discharge as observed experimentally. Alternatively, Mn displacement may take place into interstitial octahedral sites, which permits a reversible return of the Mn ion to its original site upon discharge, recovering the original Li_2MnO_2F structure and resulting in reversible O-redox without voltage loss. These new findings suggest that reversible transition metal ion migration provides a possible design route to retain the high energy density of O-redox disordered rocksalt cathodes on cycling.

INTRODUCTION

The global uptake of electric vehicles is driving demand for lithium-ion batteries with greater energy densities,[1] and hence the need for new cathodes with higher capacities.[2] Lithium-rich cathode materials with lithium/transition-metal ratios > 1, such as disordered rocksalt structured Li_2MnO_2F, and layered $Li_{1+x}(Ni,Mn,Co)O_2$ (Li-rich NMC), offer increased capacities over conventional cathodes including $LiCoO_2$ and $LiFePO_4$.[3–8] The high capacity arises because Li-rich cathodes can reversibly extract more than one Li per transition metal (TM) ion beyond the limits of conventional TM-only redox. The chemical origin of this high capacity in most Li-rich cathodes is now understood to be due to redox activity of bulk oxide ions often termed 'O-redox'.[9–11] This charge storage mechanism via the oxidation of bulk oxygen species allows Li-rich cathode materials to achieve theoretical capacities exceeding 300 mA h g^{-1} [ref [9]], opening up a new frontier in battery chemistry.

Li-rich cathodes, however, do not retain the high energy density over multiple cycles and one critical issue is that O-redox activity is almost always associated with a large hysteresis in the first-cycle voltage curve.[12–17] The hysteresis can encompass an overpotential – a kinetic effect relating to the voltage efficiency – and an irreversible loss of voltage during the first cycle.[13–21] The atomic-scale mechanisms of O-redox that contribute to the hysteresis, particularly the nature of the oxidised O species formed on charge and the role of atomic-scale rearrangements, are not well understood and remain topics of considerable debate.[22–26] For Li-rich cathodes, such as the disordered rocksalt materials, to be harnessed for technological use, the mechanisms of O-redox that contribute to the hysteresis must be identified so that strategies to mitigate the loss of energy density can be found.[27–35]

The disordered rocksalt cathode Li_2MnO_2F exhibits a large capacity comparable to that of Li-rich ordered layered oxides.[36, 37] Previous studies using resonant inelastic X-ray scattering (RIXS) and density functional theory (DFT) have identified molecular O_2 formed and trapped within the bulk structure when charged to 4.8 V (approximately $Li_{0.75}MnO_2F$), with this process associated with the additional O-redox capacity.[37] These O_2 molecules are then reversibly incorporated back into the cathode structure as O^{2-} ions on discharge. Li_2MnO_2F and some other disordered rocksalts[6, 36, 38–40] display a smaller first cycle voltage hysteresis than ordered layered counterparts,[10, 41] which raises important questions: what is the O-redox mechanism within these disordered materials at the atomic-scale, and how does their local structure facilitate a more reversible O-redox process than in Li-rich layered cathode materials? In the highly ordered Li-rich layered cathodes, it is established that TM migration is necessary for O_2 formation.[14, 16, 25, 26, 42, 43] In disordered rocksalt materials such as Li_2MnO_2F, however, it is still unclear what role, if any, TM migration plays in O_2 formation.

To address these key questions, we have conducted a study of the charge-storage mechanism in Li_2MnO_2F us-

ing DFT, X-ray absorption spectroscopy (XAS) and the galvanostatic intermittent titration technique (GITT). Our results reveal that in the highly charged (delithiated) state, molecular O_2 can form without rearrangement of the Mn framework, but that subsequent TM migration is both thermodynamically favoured and kinetically viable. We implicate irreversible Mn migration as a contributor to first-cycle voltage loss in Li_2MnO_2F, and identify a mechanism for reversible Mn migration. This work shows that allowing reversible O_2 formation, while suppressing irreversible Mn migration provides a route to stable O-redox cycling without voltage loss in the disordered rocksalt structure.

RESULTS AND DISCUSSION

Oxygen environments and short-range order in Li_2MnO_2F

Li_2MnO_2F has a disordered rocksalt crystal structure, in which octahedrally coordinated cations (Li, Mn) and anions (O, F) occupy two interpenetrating face-centred cubic (fcc) sublattices (Figure 1a). Disordered rocksalt cathodes do not display long-range order, but are known to exhibit short-range order; preferential bonding configurations and local structural motifs.[39, 44–49] Anion short range order is important to understand, because O-redox activity in Li-rich cathodes has previously been attributed to the preferential oxidation of specific lattice O^{2-} ions in Li-rich coordination environments.[50–52] O ions with a higher number of Li neighbours have a lower Madelung site potential, which lowers the energy required to localise an electron hole ($O^{2-} \rightarrow O^- + e^-$).[52] In addition, oxygen ions with linear Li–O–Li bonding configurations have O 2p states at the top of the valence band that are susceptible to oxidation on charge.[50, 51]

The potential for disordered rocksalt cathodes to exhibit extremely lithium-rich oxygen-coordination (e.g. $O-Li_6$) is particularly interesting, because removal of these Li during charging will leave these O undercoordinated with no Mn neighbours. Because the propensity for lattice O^{2-} ions to undergo oxidation is expected to be correlated with the cation coordination around each O site,[50, 52] it is important first to understand the frequency of finding O-ions in these Li-rich environments ($O-Li_6$, $O-Li_5Mn$) in the pristine Li_2MnO_2F structure.

We first used DFT calculations to parameterise a cluster-expansion Hamiltonian representing short-range interactions in Li_2MnO_2F and ran lattice Monte Carlo simulations at T = 2000 K to approximate the ball-milling synthesis conditions of the pristine, as-prepared material[36] (for computational details, see Methods). We compare the results against a model at T = ∞ K, which represents a hypothetical, fully random arrange-
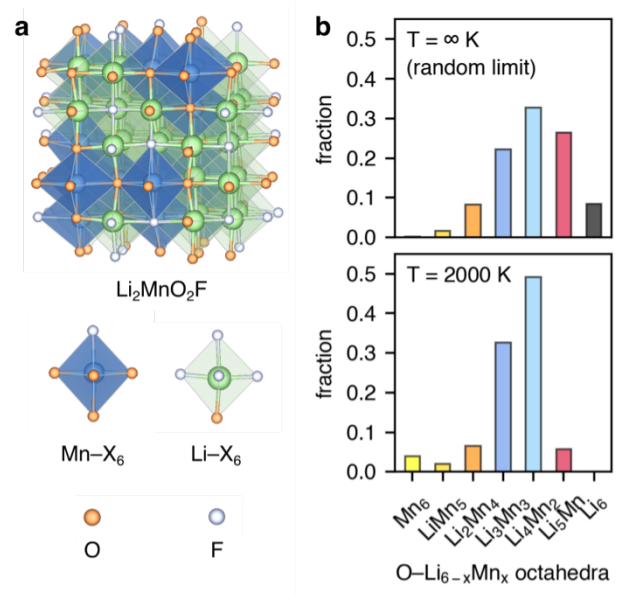

FIG. 1. Structure and short-range order of Li_2MnO_2F. (a) Representative relaxed structure of disordered Li_2MnO_2F in a (2×2×2) expansion of the conventional rocksalt unit cell. (b) Frequency of $O-Li_xMn_{6-x}$ octahedra in Li_2MnO_2F from cluster-expansion based Monte Carlo simulations at T = ∞ K (upper panel), representing the fully random limit and T = 2000 K (lower panel), representing the pristine 'as-prepared' material.

ment of the rocksalt lattice (Supplementary Note S2.1). Figure 1b shows the predicted frequencies of different O-ion coordination octahedra, $O-Li_xMn_{6-x}$, obtained by sampling structures from these Monte Carlo simulations.

Two main features emerge. First, the random limit model of Li_2MnO_2F shows a binomial distribution of $O-Li_xMn_{6-x}$ (Figure 1b). The distribution is skewed towards high Li octahedra due to the 2:1 ratio of Li/Mn in the material and 8.5% of the O-environments are $O-Li_6$. Second, in the system at T = 2000 K, the distribution of O-environments deviates from a fully random binomial distribution (Figure 1b), which indicates short-range order on the anion sublattice in pristine Li_2MnO_2F. $O-Li_6$ environments are predicted to have a very low abundance (<0.05 %), and F-ions are incorporated preferentially at anion sites with high numbers of Li neighbours (Figure S1).[46, 48] This low concentration of $O-Li_6$ environments is not sufficient to give rise to enough molecular O_2 to explain the O-redox capacity of experimental Li_2MnO_2F samples;[36, 37] the majority of the O_2 that appears on first charge must therefore originate from O that is initially bonded to at least one Mn ion (i.e., $O-Li_5Mn$, $O-Li_4Mn_2$).

Stable structures and nature of oxidised oxygen on lithium extraction

Having characterised the short-ranged order in pristine Li_2MnO_2F, we now examine the structures at high states of charge. To gain insights into the O-redox mechanism with and without the possibility of Mn migration, we considered a highly delithiated state ($Li_{0.67}MnO_2F$) using two models: a 'constrained-Mn' model and a 'mobile-Mn' model (Figure 2a). For the constrained-Mn model, we used our cluster-expansion model at T = 2000 K to generate 75 different structures, representative of the pristine material. The structures were randomly delithiated to a composition of $Li_{0.67}MnO_2F$ and relaxed with DFT, which quenches the structures to a local minimum on the potential energy surface and does not allow for significant atomic rearrangements to occur, such as Mn migration. For the mobile-Mn model, we considered 150 relaxed structures, each generated with random distributions of anions and cations plus vacancies over their respective sublattices at a composition of $Li_{0.67}MnO_2F$. The mobile-Mn model samples the full range of potential $Li_{0.67}MnO_2F$ structures that could be obtained by charging from Li_2MnO_2F if unrestricted TM and anion rearrangement were permitted. In our analysis, we focus in particular on the nature of the oxidised O species formed in these two models. For each model, we consider the distributions of O–O distances in the relaxed structures (Figure 2a); O–O distances shorter than 1.7 Å are indicative of O–O dimerisation.

The O–O interatomic distances presented in Figure 2a indicate that for the constrained-Mn model structures, we find no O-dimers of any kind. Hence charge compensation beyond the Mn^{4+} limit in these models is predominantly from localised O^- hole species on lattice ions (Supplementary Note S2.4). In contrast, the mobile-Mn structures show some O–O interatomic distances < 1.7 Å, which are a signature of covalent O–O bonds. The probability density for O–O bonds has a maximum at ~1.22 Å, indicating that molecular O_2 species are the most frequently obtained type of O-dimer.

Insight into the thermodynamics of O–O dimerisation and molecular O_2 formation in $Li_{0.67}MnO_2F$ is provided by considering the calculated energies of all the relaxed structures for the constrained-Mn and mobile-Mn models (Figure 2b). For the mobile-Mn structures we classify these data according to whether a given structure contains a covalent O–O bond. The distribution of energies for each set of structures reveals two key details. First, the mobile-Mn structures that contain covalent O–O bonds are on average significantly lower in energy (~0.4 eV f.u.$^{-1}$) than those that do not contain covalent O–O bonds, and also lower in energy on average than the constrained-Mn set of structures. We further classify the structures containing O–O bonds depending on the O–O bond length and thus the type of
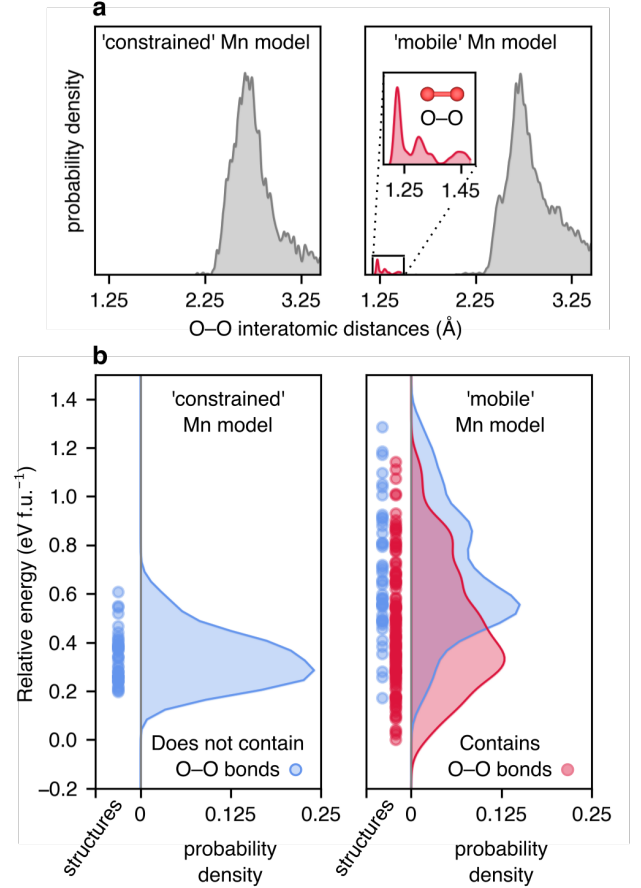

FIG. 2. Search for O–O bonds and thermodynamics of O-dimer formation in delithiated $Li_{0.67}MnO_2F$. (a) Search for O–O dimers by an analysis O–O interatomic distances in delithiated structures of the pristine material obtained from the cluster-expansion ('constrained' Mn), and in 'mobile' Mn models. (b) Energetics of the structures from (a) with the structures from the 'mobile' Mn model separated into those containing O–O bonds (< 1.7 Å) and those not containing O–O bonds. The right section of each panels shows the kernel density estimations of the probability of energies in the left panel, where each dot is the energy of a structure.

O–dimer; peroxide, superoxide or molecular O_2 (Supplementary Note S2.3). We find that structures containing molecular O_2 are on average, the most stable (Figure S2). These results therefore show a strong thermodynamic driving force for the formation of molecular O_2 at high states of charge ($Li_{0.67}MnO_2F$); the constrained-Mn structures, in which charge-compensation beyond the Mn^{4+} limit is purely through localised oxygen holes on lattice oxide ions, are metastable. Second, direct examination of the corresponding starting structures shows that these molecular O_2 species form exclusively from oxygen initially in $O-Li_6$ environments. This result indicates that, if starting from pristine Li_2MnO_2F with very few $O-Li_6$ environments, full oxidation of lattice oxide ions to form molecular O_2 is an activated process

requiring Mn–O bond breaking. This process is expected to be associated with a rearrangement of the TM framework, as has been proposed previously for ordered Li-rich cathodes.[14, 16, 18, 25, 43, 53]
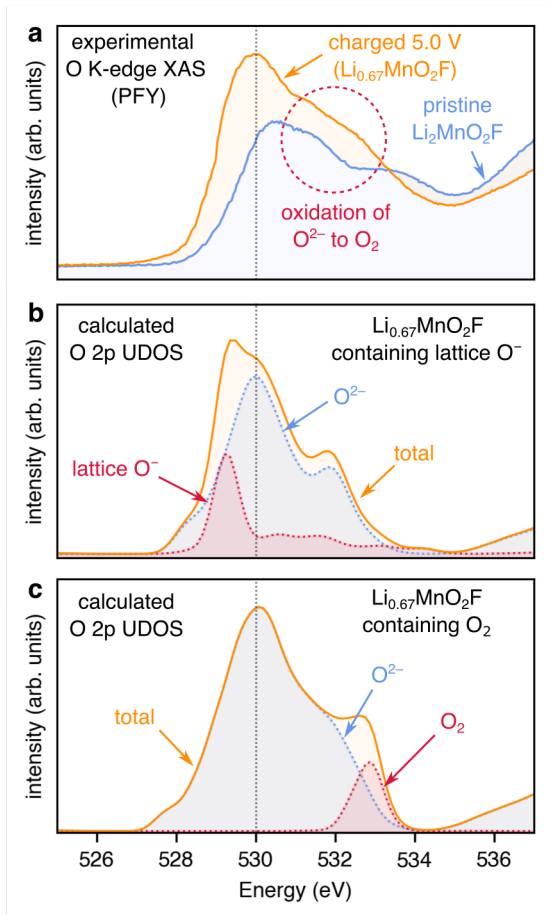

FIG. 3. Electronic structure properties of pristine Li_2MnO_2F and delithiated $Li_{0.67}MnO_2F$. (a) Experimental O K-edge XAS in bulk-sensitive partial fluorescence yield (PFY) mode for pristine Li_2MnO_2F and the material charged to 5.0 V (approximately $Li_{0.67}MnO_2F$). (b) Calculated unoccupied O 2p density of states (UDOS) for delithiated ($Li_{0.67}MnO_2F$) structures containing lattice O^- holes. (c) Calculated UDOS for $Li_{0.67}MnO_2F$ structures containing O_2. The UDOS are aligned for each individual O atom with respect to the O 1s level, giving an approximation of the O K-edge XAS spectrum (see Methods).

The extent to which oxidised lattice O species, sometimes termed 'lattice oxygen redox', contribute to charge compensation in O-redox cathodes has been widely debated.[24, 42, 54–57] Recent studies using O K-edge X-ray absorption spectroscopy (XAS) and post-DFT calculations show that oxidised lattice O species in Mn-based cathodes appear as a distinct feature in the XAS spectrum, below the main pre-edge peak.[16, 58]

To investigate whether any localised holes states on O are experimentally observed, we calculated the elec-

tronic structure properties of pristine and delithiated Li_2MnO_2F, and compared these with experimentally observed features in the O K-edge X-ray absorption spectrum (Supplementary Note S4). The O 2p unoccupied density of states (UDOS), aligned for each O atom with respect to the O 1s level, provide insights into the unoccupied states and the O K-edge spectral features.

The experimental O K-edge XAS are shown in Figure 3a. Upon charging to 5 V (approximately $Li_{0.67}MnO_2F$), the main pre-edge feature shifts from ~530.5 eV to ~530.0 eV, indicating oxidation of Mn from 3+ to 4+. In addition, there is increased intensity in the region at ~531–532 eV, above the main pre-edge feature,[36] which has been associated with O-redox. The calculated UDOS for the metastable charged $Li_{0.67}MnO_2F$ structure (Figure 3b), which displays charge-compensation purely through localised holes on lattice O-ions, shows a new feature at ~529 eV, due to these hole species, resulting in a distinct shoulder below the main 530 peak.[16, 58] The calculated feature at ~529 eV is absent from the experimental O K-edge XAS spectrum, suggesting that localised oxygen holes do not persist in the real material.

The UDOS for the $Li_{0.67}MnO_2F$ structure containing molecular O_2 (Figure 3c) shows a new feature at 533 eV, from empty orbitals on the O atoms of the O_2 molecules; this feature is consistent with experimental observation of increased intensity in the region above the main pre-edge peak at 530 eV.[36] Crucially, unoccupied O 2p states appearing above the main pre-edge feature at the O K edge (~531 eV) can not arise from lattice O^{n-} ions, and instead arise when major structural rearrangements have taken place that allow covalent O bonding, such as for molecular O_2 species.[58] In short, our results indicate that charge-compensation beyond the Mn^{4+} redox limit is achieved through O_2 formation, and not through localised holes on lattice O ions.

Mechanism of O–O dimerisation in the delithiated material

The results above show that there is a strong thermodynamic driving force for O_2 formation accommodated by Mn migration in the delithiated material $Li_{0.67}MnO_2F$ which is consistent with the experimental observation of molecular O_2 formation trapped in the bulk structure.[37] However, the precise kinetic barriers for each of these processes are still unclear.

To investigate the energetics of O_2 formation in the delithiated material in greater detail, we have calculated the activation barrier for O–O dimerisation using the nudged elastic band method (Figure 4). We started with a metastable $Li_{0.67}MnO_2F$ structure by removing Li from a representative pristine structure (Supplementary Note S2.5). At this high level of delithiation, some O–ions that were in Li-rich environments (i.e., $O-Li_5Mn$,
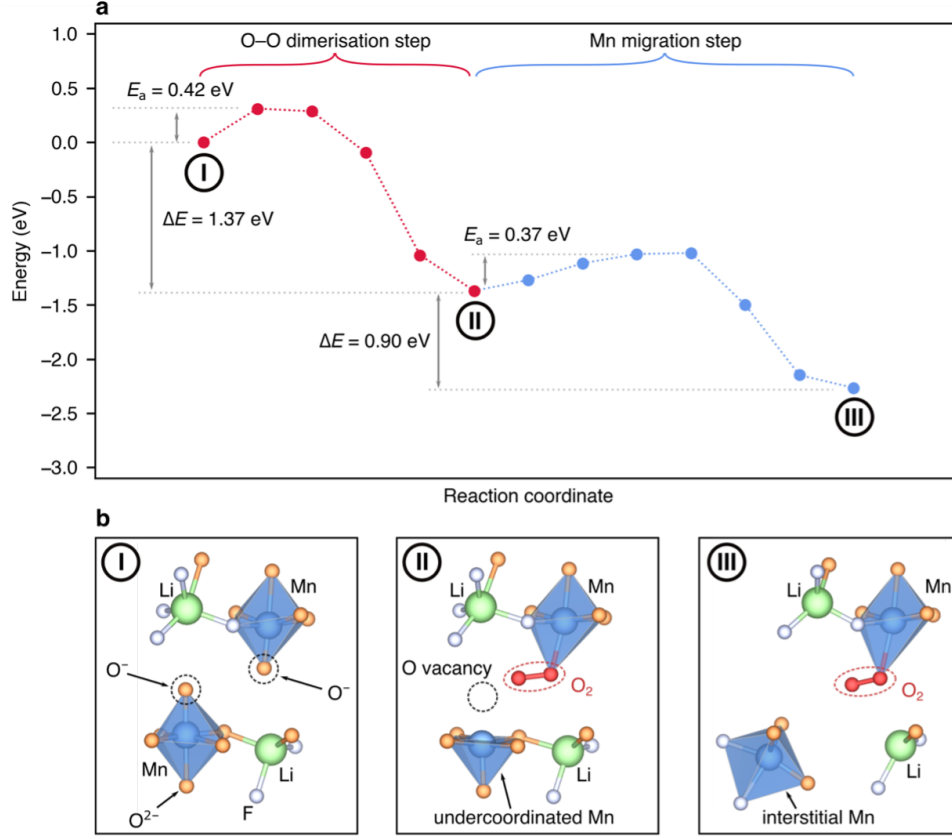
FIG. 4. Reaction mechanism to form O–O dimers in $Li_{0.67}MnO_2F$. (a) Energetics of structures along a reaction pathway to form O–O in $Li_{0.67}MnO_2F$ obtained from nudged elastic band (NEB) calculations. (b) Key optimised structures along the reaction pathway in (a).

$O-Li_4Mn_2$) in the pristine material now display localised oxygen holes (formally O^-). As discussed above, this structure is metastable, and favours the formation of O_2, which starts with the direct interaction of two adjacent O^- ions at $O-Li_{5-x}Mn$ sites (x > 2) (shown as structure I in Figure 4). O–O dimerisation proceeds by detachment of one of the O^- ions from its Mn neighbour,[59] overcoming an activation barrier of 0.4 eV, and forming molecular O_2 trapped in the bulk (structure II). This first step stabilises the structure by –1.37 eV. The first step also creates an oxygen vacancy at the original $O-Li_{5-x}Mn$ site, leaving the Mn ion in an undercoordinated 5-fold geometry (Figure 4b, structure II).

We then investigated the migration of the undercoordinated Mn to a new octahedral site, obtaining structure III. The activation barrier for this step is 0.37 eV, and the structure is stabilised by –0.9 eV. At the end of this pathway, the Mn ion relaxes into an interstitial site, where the Mn ion resides in a distorted octahedral position, located where the shared edge of two octahedra would be in the pristine rocksalt structure (Figure 4b, Figure 5c). This position can be occupied under these circumstances due to large displacements of the anions

in highly delithiated $Li_{0.67}MnO_2F$, relative to their positions on the perfect rocksalt anion sublattice, illustrated in Figure 5. In pristine, as-synthesised Li_2MnO_2F, the anions show small deviations ($\sim$0.125 Å) away from the perfect rocksalt sublattice, due to Jahn-Teller distortions of Mn^{3+} ions. Since the deviations are small, interstitial positions cannot be occupied by cations due to short TM–O distances (< 1.5 Å) and high electrostatic repulsion from cation-cation face-sharing polyhedra. At high levels of delithiation, however, the removal of Li result in local relaxations of the O and F ions of up to 1 Å (Figure 5d). This significant disruption to the anion sublattice allows Mn ions to adopt octahedral coordination in new interstitial sites.

Having demonstrated that Mn migration is possible, we continued along the same reaction pathway by examining additional Mn migration steps away from the vacancy cluster containing O_2 to form a structure that contains two O_2 molecules (Figure S5). These O_2 molecules exist in an Mn-deficient 'nanovoid', itself formed by Mn migration away from the original site where the first O_2 molecule formed. In the structure containing the two O_2 molecules, both O–O distances are 1.23 Å. We have
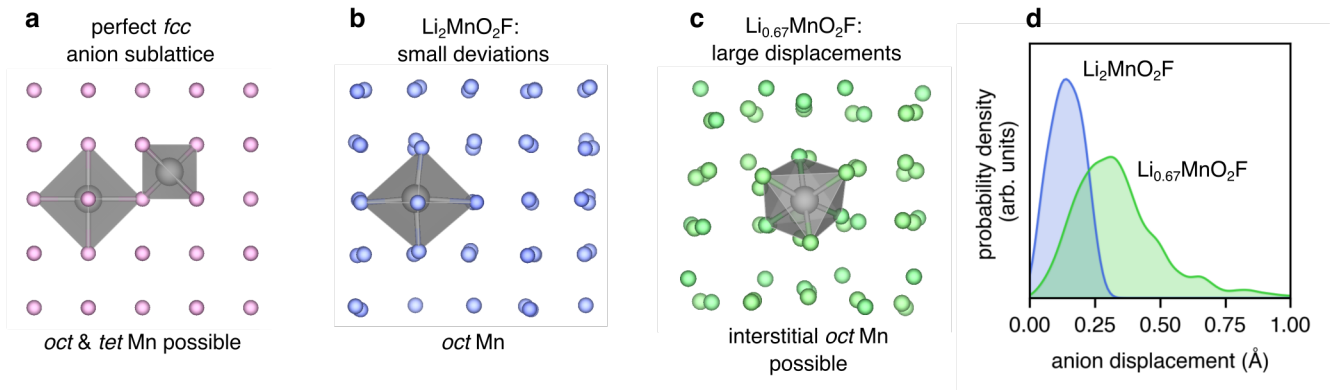
FIG. 5. Off-site deviations and displacements in the rocksalt anion sublattice. (a) A perfect fcc anion sublattice features octahedral tetrahedral cation sites. (b) Jahn-Teller distorted Mn ions in Li_2MnO_2F result in small off-lattice anion deviations. (c) Delithiation to $Li_{0.67}MnO_2F$ causes large off-lattice displacements, and permits cations to occupy 'interstitial' octahedral sites. (d) Calculated magnitude of off-lattice displacements for all anions in structures of Li_2MnO_2F and $Li_{0.67}MnO_2F$, presented as normalised probability density plots. The distribution for Li_2MnO_2F was obtained from 25 relaxed structures from the cluster-expansion model at 2000 K, and the results for $Li_{0.67}MnO_2F$ were obtained from the 75 structures of the 'constrained-Mn' model.

performed ab initio molecular dynamics (AIMD) simulations to examine any mobility of the O_2 molecules in the nanovoid, as well as the dynamic nature of the O–O bonds. Over the simulation timescale, the average O–O bond lengths are close to 1.23 Å (Figure S6) and the vibrational frequencies are 1550 cm^{-1} (Figure S5); these results are in good agreement with the experimental values reported for molecular O_2 from ex situ RIXS measurements of charged $Li_{0.75}MnO_2F$.[37] Similar TM deficient regions have also been observed experimentally in disordered rocksalt $Li_{1.3}Nb_{0.3}Fe_{0.4}O_2$ from transmission electron microscopy (TEM),[23] and in Li-rich nickel-manganese-cobalt oxide (Li-rich NMC) and $Li_{1.2}Mn_{0.6}Ni_{0.2}O_2$ from small-angle X-ray scattering (SAXS),[60] and other studies,[8, 61] although scattering experiments have not yet been able to detect O_2 molecules.

Charge-discharge process and voltage hysteresis

Understanding the relationship between voltage hysteresis, TM migration and O_2 formation in Li-rich cathodes requires investigating both the charge and discharge processes. For example, in ordered Li-rich NMC, the large voltage hysteresis has been linked to molecular O_2 formation, which drives a disordering of the cations during the high-voltage charge plateau, and results in a new structure upon discharge.[14] By contrast, in disordered Li_2MnO_2F, the voltage hysteresis is much smaller than for Li-rich NMC, and no major structural changes have been detected experimentally over the first charge-discharge cycle.[36, 37] Our results show, however, that in Li_2MnO_2F molecular O_2 formation does indeed drive
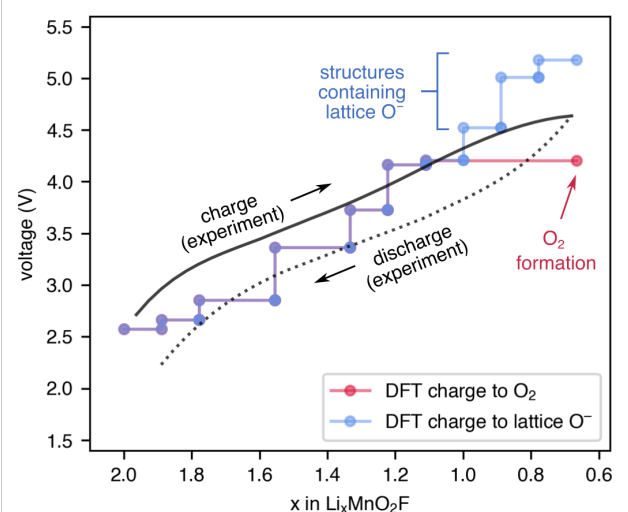

FIG. 6. Experimental and calculated voltage curves. The calculations are based on charging to structures containing lattice O^- (Figure S7), or to structures containing O_2, compared against the experimental first-cycle voltage-capacity curve from GITT measurements.

a change to the cathode host framework at the top of charge, which may influence the structure after the first cycle.

To investigate the voltage hysteresis, we calculated the voltage curve upon charging to $Li_{0.67}MnO_2F$, either to metastable structures containing lattice O^- or to structures containing O_2, which involve a re-arrangement of the Mn framework (Figure 6). The calculated charge voltage curves were compared with an experimental charge curve obtained from GITT measurements (see Methods). We then investigated the discharge pro-
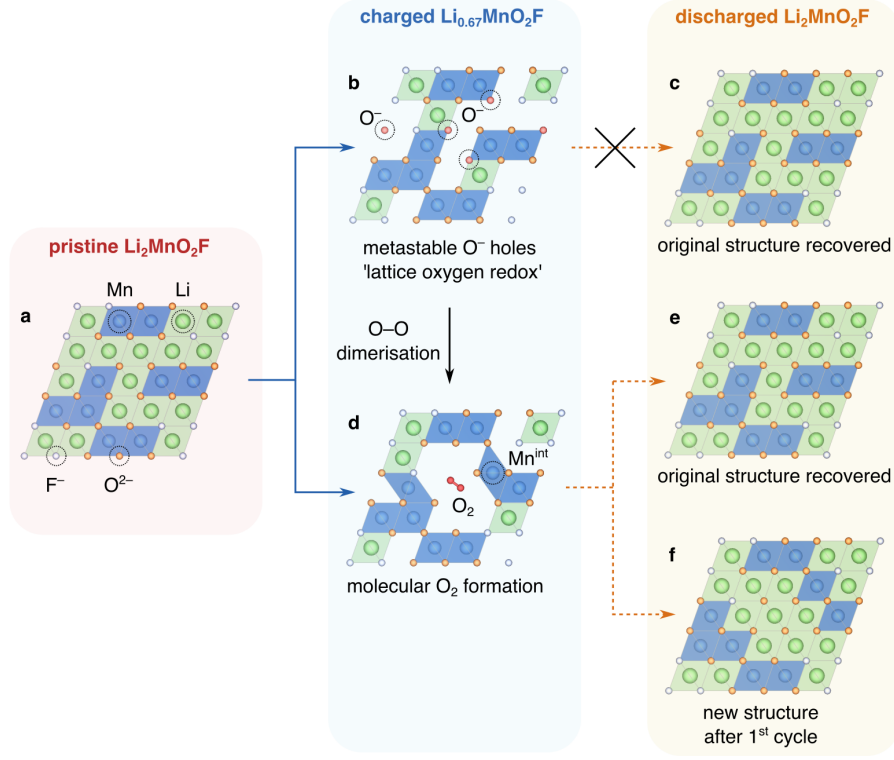
FIG. 7. Possible pathways for the charge-discharge process and voltage hysteresis. (a) Pristine Li_2MnO_2F structure, (b) charged structure with metastable lattice O^- holes, (c) re-inserting Li on discharge recovers the original structure. (d) O^- holes dimerise to form molecular O_2, with Mn ions displaced into interstitial sites. From structure (d), on discharge, there are two possible pathways that can occur. (e) Reversible migration of Mn back to its original site, recovers the original structure. This process results in a kinetic (overpotential) voltage hysteresis, but no voltage fade. (f) Mn ions irreversibly migrate to new octahedral sites resulting in a new structure on discharge, involving a voltage hysteresis during the first cycle.

cess following structural rearrangement, by re-inserting lithium ions back into structure containing O_2 and calculating the average discharge voltage.

As already revealed, when the structure is charged beyond the limit of Mn^{3+} to Mn^{4+} redox, structures containing lattice O^- are metastable with respect to O_2 formation (Figure 2). The calculated charge voltage curve to structures containing lattice O^- exceeds 5 V, clearly inconsistent with experiment (Figure 6). The calculated delithiated structure containing O_2 occurs at a lower voltage, providing a better agreement with experiment. The average charge voltage from the pristine structure to the structure containing O_2 is 3.53 V. Upon discharge, reinserting Li into the structure containing O_2, a new discharged structure is obtained containing two $O-Li_6$ environments, where the O atoms of the O_2 molecule are re-incorporated into the lattice. This new discharged structure is significantly higher in energy ($\sim$0.4 eV f.u.$^{-1}$) than the pristine Li_2MnO_2F structure, due to the relative instability of the trapped $O-Li_6$ environments (Figure S7). The average discharge voltage is 3.22 V, lower than the charge voltage; i.e., there is a voltage hysteresis, arising from the irreversible structural transformation to

form O_2.

Our results provide insight into the smaller first-cycle voltage hysteresis for some Li-rich disordered rocksalt cathodes, such as Li_2MnO_2F, compared to ordered counterparts such as Li-rich NMC.[14, 36] The layered structure of Li-rich NMC has honeycomb ordered Li and all O ions are coordinated to at least two TM ions ($O-Li_{4-x}TM_2$). Upon delithiation of Li-rich NMC, the TM ions become susceptible to migration to adjacent octahedral vacancies in the TM layer or interlayer space,[26, 62] allowing O_2 formation to take place.[14] The overall effect is a large-scale disordering of the cations in the structure, leading to a discharged structure with more $O-Li_5TM$ and $O-Li_6$ environments than in the pristine materials and consequently a lower voltage on charge for the second cycle.

By contrast, in the Li-rich disordered rocksalts, some O ions are coordinated to only a single Mn ion ($O-Li_{5-x}Mn$). When delithiation passes the limits of TM redox with O_2-formation, these $O-Li_{5-x}Mn$ ions are the first to be oxidised to O^-, and are likely to be the sites where O_2 formation can most easily occur (Figure 7b). Such oxygen vacancies at $O-Li_{5-x}Mn$ sites will leave only

a single Mn ion undercoordinated, which means fewer Mn ions must migrate to new sites to stabilise the structure. Overall, O_2 formation in disordered rocksalts will drive less of a structural rearrangement on the first cycle than ordered layered O-redox cathodes.

Furthermore, the mechanism of reversible Mn migration, possible in $Li_{2-x}MnO_2F$ due to the large off-lattice anion displacements at the top of charge, and Mn displacement into interstitial sites, provides a pathway to O-redox with a reduced voltage hysteresis and without voltage fade. If Mn migration is fully reversible, the O atoms of the O_2 will return to their original O coordination after discharge, and the original structure is recovered. There will be a thermodynamic driving force for such a process during discharge, due to the greater stability of the original Li_2MnO_2F structure relative to the discharged structure containing $O-Li_6$ environments (Figure S7). Fully reversible Mn migration will result in a hysteresis associated with the kinetics of the Mn migration and O_2 formation process, and will not result in voltage fade.

Discussion: strategies to harness reversible O-redox

Preventing voltage hysteresis and voltage fade is critical for technological implementation of O-redox cathodes with high energy densities. Voltage hysteresis in ordered Li-rich cathodes has previously been linked to bulk TM migration during charging, evident from a loss of layering or ordering from average structure techniques (i.e. X-ray diffraction [XRD]) and imaging (i.e., transmission electron microscopy).[14, 16, 25, 26] In contrast, evidence for bulk TM migration in disordered rocksalt cathodes is limited and has been much more challenging to observe directly. TM migration, however, has been identified in some disordered rocksalt cathodes from XRD,[15, 63] and local structural probes.[46, 64, 65] Our study presents evidence that O–O dimerisation provides a thermodynamic driving force for irreversible TM migration in Li-rich disordered rocksalt cathodes. In charged Li_2MnO_2F, O–O dimerisation leads to undercoordinated (5-fold) Mn which is then stabilised by migrating to a new fully coordinated octahedral site. Irreversible Mn migration leads to a voltage hysteresis and a different structure after the first cycle.

As discussed previously,[22] a possible strategy to suppress the voltage hysteresis in O-redox cathodes is to prevent O_2 formation by inhibiting TM migration; i.e., kinetically trapping the charged structures in a metastable state with bulk localised, 'split-polaron' or delocalised O-holes.[16, 58, 66] We suggest that this strategy is unlikely to be effective in Li_2MnO_2F because of relatively easy Mn migration. This is a two-fold effect, related to the high Li:TM ratio in Li_2MnO_2F. Firstly, a high concentration of Li will simply allow many possible vacant cation sites

for Mn to migrate into on Li extraction. Secondly, removing a high fraction of Li from the structure will lead to significant local relaxations of the host framework, including off-lattice anion displacements discussed above, resulting in low activation barriers ($\sim$0.45 eV) for some Mn migration pathways. Such low activation barriers for TM migration pathways will make it challenging to suppress TM migration, and thus difficult to prevent voltage hysteresis.

The link between high Li:TM ratios and ease of Mn migration implies a trade-off in disordered rocksalt cathodes between theoretical capacity and preventing voltage hysteresis. Lower levels of Li-excess, and a more continuous and connected 3D framework of edge-sharing TM-ions is expected to help prevent TM migration. A similar principle has been proposed in layered Li-rich cathodes, where the superstructure ordering within TM layers affects the stability of those layers; greater stability is achieved with more continuous TM connectivity.[16] Interesting 3D examples are 'partially ordered' spinel-type Mn-oxyfluoride cathodes, which display small voltage hysteresis.[40] These materials have a relatively low Li/TM ratio ($\sim$1.5), and defect-spinel structure, with well-connected network of edge-sharing Mn octahedra. We suggest that these features will tend to reduce the magnitude of off-lattice anion displacements, and inhibit TM migration. Achieving a lower level of Li-excess in Li_2MnO_2F, if the level of fluorination is kept constant, opens the possibility of using low-valent dopants such as Mg^{2+} and Zn^{2+},[67] in contrast to high-valent d^0 dopants such as Ti^{4+} and Nb^{5+} that are often used in disordered rocksalt cathodes.[41]

An alternative approach to the design of Li-rich disordered rocksalt cathodes will be to allow O_2 formation and then aim to achieve O–O dimerisation with reversible TM migration while preventing irreversible TM migration.[22] By allowing O_2 formation, the cathode is rendered much more stable on charge, since unstable lattice O^- species are not trapped in the structure. To suppress irreversible TM migration, the displacement of Mn into interstitial sites is important because the Mn can return to their original sites on discharge. Similarly, the displacement of octahedral cations into tetrahedral sites, as has recently been described for $Cr^{3+} \rightarrow Cr^{6+}$ in the disordered rocksalt cathodes $Li_{1.2}Mn_{0.2}Ti_{0.4}Cr_{0.2}O_2$ [ref[65]] and $Li_2Mn_{0.75}Cr_{0.25}O_2F$ [ref[68]] may permit O–O dimerisation while fully or partially recovering the original structure on discharge.

CONCLUSIONS

This study has revealed important insights into the O-redox mechanism and voltage hysteresis in the disordered rocksalt cathode Li_2MnO_2F including the role of transition metal migration. We have shown that on delithia-

tion charge-compensation beyond the Mn^{4+} redox limit is not achieved through localised holes on lattice oxide ions, and occurs instead through molecular O_2 formation. On charge, metastable O^- ions dimerise to form O_2 trapped within lithium vacancy clusters or nanovoids of the bulk material leaving oxygen vacancies at undercoordinated (5-fold) Mn ions. Subsequently, these undercoordinated Mn ions move into fully coordinated octahedral interstitial sites. Such Mn displacement can take place in two ways. When migration is irreversible, the coordination around O^{2-} changes, which leads to a lower voltage on discharge than on charge (voltage hysteresis) in agreement with experimental observations. Alternatively, if Mn displacement is reversible, whereby the Mn ion returns to its original site upon discharge, the original Li_2MnO_2F structure and coordination around O^{2-} is recovered, which facilitates reversible O-redox without voltage hysteresis. In both cases, the O_2 molecules are reduced back to lattice O^{2-} ions on discharge. The results presented here suggest that reversible transition metal displacement provides a strategy to harness O-redox in Li-rich disordered rocksalt cathode materials without loss of their high energy density.

CONFLICTS OF INTEREST

There are no conflicts to declare.

ACKNOWLEDGEMENTS

---

* m.s.islam@bath.ac.uk

[1] Y. Liu, Y. Zhu and Y. Cui, *Nature Energy*, 2019, **4**, 540–550.

[2] P. Rozier and J. M. Tarascon, *Journal of The Electrochemical Society*, 2015, **162**, A2490–A2499.

[3] X. Li, Y. Qiao, S. Guo, K. Jiang, M. Ishida and H. Zhou, *Advanced Materials*, 2019, **31**, 1807825.

[4] M. J. Crafton, Y. Yue, T.-Y. Huang, W. Tong and B. D. McCloskey, *Advanced Energy Materials*, 2020, **10**, 2001500.

[5] I. Källquist, A. J. Naylor, C. Baur, J. Chable, J. Kullgren, M. Fichtner, K. Edström, D. Brandell and M. Hahlin, *Chemistry of Materials*, 2019, **31**, 6084–6096.

[6] R. Chen, S. Ren, M. Knapp, D. Wang, R. Witter, M. Fichtner and H. Hahn, *Advanced Energy Materials*, 2015, **5**, 1401814.

[7] N. Yabuuchi, M. Takeuchi, M. Nakayama, H. Shiiba, M. Ogawa, K. Nakayama, T. Ohta, D. Endo, T. Ozaki, T. Inamasu, K. Sato and S. Komaba, *Proceedings of the National Academy of Sciences*, 2015, **112**, 7650.

[8] E. Hu, X. Yu, R. Lin, X. Bi, J. Lu, S. Bak, K.-W. Nam, H. L. Xin, C. Jaye, D. A. Fischer, K. Amine and X.-Q. Yang, *Nature Energy*, 2018, **3**, 690–698.

[9] G. Assat and J.-M. Tarascon, *Nature Energy*, 2018, **3**, 373–386.

[10] N. Yabuuchi, *The Chemical Record*, 2019, **19**, 690–707.

[11] M. Ben Yahia, J. Vergnet, M. Saubanère and M.-L. Doublet, *Nature Materials*, 2019, **18**, 496–502.

[12] J. R. Croy, K. G. Gallagher, M. Balasubramanian, B. R. Long and M. M. Thackeray, *Journal of The Electrochemical Society*, 2013, **161**, A318–A325.

[13] Q. Jacquet, A. Iadecola, M. Saubanère, H. Li, E. J. Berg, G. Rousse, J. Cabana, M.-L. Doublet and J.-M. Tarascon, *Journal of the American Chemical Society*, 2019, **141**, 11452–11464.

[14] R. A. House, G. J. Rees, M. A. Pérez-Osorio, J.-J. Marie, E. Boivin, A. W. Robertson, A. Nag, M. Garcia-Fernandez, K.-J. Zhou and P. G. Bruce, *Nature Energy*, 2020, **5**, 777–785.

[15] B. Li, M. T. Sougrati, G. Rousse, A. V. Morozov, R. Dedryvère, A. Iadecola, A. Senyshyn, L. Zhang, A. M. Abakumov, M.-L. Doublet and J.-M. Tarascon, *Nature Chemistry*, 2021.

[16] R. A. House, U. Maitra, M. A. Pérez-Osorio, J. G. Lozano, L. Jin, J. W. Somerville, L. C. Duda, A. Nag, A. Walters, K.-J. Zhou, M. R. Roberts and P. G. Bruce, *Nature*, 2020, **577**, 502–508.

[17] Z. N. Taylor, A. J. Perez, J. A. Coca-Clemente, F. Braga, N. E. Drewett, M. J. Pitcher, W. J. Thomas, M. S. Dyer, C. Collins, M. Zanella, T. Johnson, S. Day, C. Tang, V. R. Dhanak, J. B. Claridge, L. J. Hardwick and M. J. Rosseinsky, *Journal of the American Chemical Society*, 2019, **141**, 7333–7346.

[18] J. Vinckeviciute, D. A. Kitchaev and A. Van der Ven, *Chemistry of Materials*, 2021, **33**, 1625–1636.

[19] G. Assat, S. L. Glazier, C. Delacourt and J.-M. Tarascon, *Nature Energy*, 2019, **4**, 647–656.

[20] G. Assat, D. Foix, C. Delacourt, A. Iadecola, R. Dedryvère and J.-M. Tarascon, *Nature Communications*, 2017, **8**, 2219.

[21] Z. Yu, F. Ning, H. Shang, J. Song, T. Yao, Z. Sun, W. Chu and D. Xia, *The Journal of Physical Chemistry C*, 2021, **125**, 16913–16920.

[22] R. A. House, J.-J. Marie, M. A. Pérez-Osorio, G. J. Rees, E. Boivin and P. G. Bruce, *Nature Energy*, 2021.

[23] N. Yabuuchi, M. Nakayama, M. Takeuchi, S. Komaba, Y. Hashimoto, T. Mukai, H. Shiiba, K. Sato, Y. Kobayashi, A. Nakao, M. Yonemura, K. Yamanaka, K. Mitsuhara and T. Ohta, *Nature Communications*, 2016, **7**, 13814.

[24] M. D. Radin, J. Vinckeviciute, R. Seshadri and A. Van der Ven, *Nature Energy*, 2019, **4**, 639–646.

[25] J. Hong, W. E. Gent, P. Xiao, K. Lim, D.-H. Seo, J. Wu, P. M. Csernica, C. J. Takacs, D. Nordlund, C.-J. Sun, K. H. Stone, D. Passarello, W. Yang, D. Prendergast, G. Ceder, M. F. Toney and W. C. Chueh, *Nature Materials*, 2019, **18**, 256–265.

[26] W. E. Gent, K. Lim, Y. Liang, Q. Li, T. Barnes, S.-J. Ahn, K. H. Stone, M. McIntire, J. Hong, J. H. Song, Y. Li, A. Mehta, S. Ermon, T. Tyliszczak, D. Kilcoyne, D. Vine, J.-H. Park, S.-K. Doo, M. F. Toney, W. Yang, D. Prendergast and W. C. Chueh, *Nature Communications*, 2017, **8**, 2091.

[27] C. Baur, I. Källquist, J. Chable, J. H. Chang, R. E. Johnsen, F. Ruiz-Zepeda, J.-M. Ateba Mba, A. J. Naylor, J. M. Garcia-Lastra, T. Vegge, F. Klein, A. R. Schür, P. Norby, K. Edström, M. Hahlin and M. Fichtner, *Journal of Materials Chemistry A*, 2019, **7**, 21244–21253.

[28] Yao Z., Kim S., He J., Hegde V. I. and Wolverton C., *Science Advances*, **4**, eaao6754.

[29] Y. Yue, N. Li, L. Li, E. E. Foley, Y. Fu, V. S. Battaglia, R. J. Clément, C. Wang and W. Tong, *Chemistry of Materials*, 2020, **32**, 4490–4498.

[30] J. H. Chang, C. Baur, J.-M. Ateba Mba, D. Arčon, G. Mali, D. Alwast, R. J. Behm, M. Fichtner, T. Vegge and J. M. Garcia Lastra, *Journal of Materials Chemistry A*, 2020, **8**, 16551–16559.

[31] D. Chen, W. H. Kan and G. Chen, *Advanced Energy Materials*, 2019, **9**, 1901255.

[32] Y. Yue, N. Li, Y. Ha, M. J. Crafton, B. D. McCloskey, W. Yang and W. Tong, *Advanced Functional Materials*, 2021, **31**, 2008696.

[33] H. Chung, Z. Lebens-Higgins, B. Sayahpour, C. Mejia, A. Grenier, G. E. Kamm, Y. Li, R. Huang, L. F. J. Piper, K. W. Chapman, J.-M. Doux and Y. S. Meng, *Journal of Materials Chemistry A*, 2021, **9**, 1720–1732.

[34] H. Lee, W. Choi, W. Lee, J.-H. Shim, Y.-M. Kim and W.-S. Yoon, *Advanced Energy Materials*, 2021, **11**, 2002958.

[35] A. J. Naylor, I. Källquist, D. Peralta, J.-F. Martin, A. Boulineau, J.-F. Colin, C. Baur, J. Chable, M. Fichtner, K. Edström, M. Hahlin and D. Brandell, *ACS Applied Energy Materials*, 2020, **3**, 5937–5948.

[36] R. A. House, L. Jin, U. Maitra, K. Tsuruta, J. W. Somerville, D. P. Förstermann, F. Massel, L. Duda, M. R. Roberts and P. G. Bruce, *Energy Environ. Sci.*, 2018, **11**, 926–932.

[37] R. Sharpe, R. A. House, M. J. Clarke, D. Förstermann, J.-J. Marie, G. Cibin, K.-J. Zhou, H. Y. Playford, P. G. Bruce and M. S. Islam, *Journal of the American Chemical Society*, 2020, **142**, 21799–21809.

[38] J. Lee, D. A. Kitchaev, D.-H. Kwon, C.-W. Lee, J. K. Papp, Y.-S. Liu, Z. Lun, R. J. Clément, T. Shi, B. D. McCloskey, J. Guo, M. Balasubramanian and G. Ceder, *Nature*, 2018, **556**, 185–190.

[39] Z. Lun, B. Ouyang, Z. Cai, R. J. Clément, D.-H. Kwon, J. Huang, J. K. Papp, M. Balasubramanian, Y. Tian, B. D. McCloskey, H. Ji, H. Kim, D. A. Kitchaev and G. Ceder, *Chem*, 2020, **6**, 153–168.

[40] H. Ji, J. Wu, Z. Cai, J. Liu, D.-H. Kwon, H. Kim, A. Urban, J. K. Papp, E. Foley, Y. Tian, M. Balasubramanian, H. Kim, R. J. Clément, B. D. McCloskey, W. Yang and G. Ceder, *Nature Energy*, 2020, **5**, 213–221.

[41] R. J. Clément, Z. Lun and G. Ceder, *Energy Environ. Sci.*, 2020, **13**, 345–373.

[42] W. E. Gent, I. I. Abate, W. Yang, L. F. Nazar and W. C. Chueh, *Joule*, 2020, **4**, 1369 – 1397.

[43] E. Boivin, R. A. House, M. A. Pérez-Osorio, J.-J. Marie, U. Maitra, G. J. Rees and P. G. Bruce, *Joule*, 2021, **5**, 1267–1280.

[44] R. J. Clément, Z. Lun and G. Ceder, *Energy Environ. Sci.*, 2020, **13**, 345–373.

[45] H. Ji, A. Urban, D. A. Kitchaev, D.-H. Kwon, N. Artrith, C. Ophus, W. Huang, Z. Cai, T. Shi, J. C. Kim, H. Kim and G. Ceder, *Nature Communications*, 2019, **10**, 592.

[46] R. J. Clément, D. Kitchaev, J. Lee and G. Ceder, *Chemistry of Materials*, 2018, **30**, 6945–6956.

[47] N. Mozhzhukhina, J. Kullgren, C. Baur, O. Gustafsson, W. R. Brant, M. Fichtner and D. Brandell, *Journal of Raman Spectroscopy*, 2020, **51**, 2095–2101.

[48] B. Ouyang, N. Artrith, Z. Lun, Z. Jadidi, D. A. Kitchaev, H. Ji, A. Urban and G. Ceder, *Advanced Energy Materials*, 2020, **10**, 1903240.

[49] W. D. Richards, S. T. Dacek, D. A. Kitchaev and G. Ceder, *Advanced Energy Materials*, 2018, **8**, 1701533.

[50] D.-H. Seo, J. Lee, A. Urban, R. Malik, S. Kang and G. Ceder, *Nature Chemistry*, 2016, **8**, 692–697.

[51] K. Luo, M. R. Roberts, R. Hao, N. Guerrini, D. M. Pickup, Y.-S. Liu, K. Edström, J. Guo, A. V. Chadwick, L. C. Duda and P. G. Bruce, *Nature Chemistry*, 2016, **8**, 684–691.

[52] D. W. Davies, B. J. Morgan, D. O. Scanlon and A. Walsh, *IOP SciNotes*, 2020, **1**, 024805.

[53] Z. Zhang, S. Zhao, B. Wang and H. Yu, *Cell Reports Physical Science*, 2020, **1**, 100061.

[54] J. Wu, Z. Zhuo, X. Rong, K. Dai, Z. Lebens-Higgins, S. Sallis, F. Pan, L. F. J. Piper, G. Liu, Y.-d. Chuang, Z. Hussain, Q. Li, R. Zeng, Z.-x. Shen and W. Yang, *Science Advances*, 2020, **6**, eaaw3871.

[55] J. Xu, M. Sun, R. Qiao, S. E. Renfrew, L. Ma, T. Wu, S. Hwang, D. Nordlund, D. Su, K. Amine, J. Lu, B. D. McCloskey, W. Yang and W. Tong, *Nature Communications*, 2018, **9**, 947.

[56] Y. Yu, P. Karayaylali, S. H. Nowak, L. Giordano, M. Gauthier, W. Hong, R. Kou, Q. Li, J. Vinson, T. Kroll, D. Sokaras, C.-J. Sun, N. Charles, F. Maglia, R. Jung and Y. Shao-Horn, *Chemistry of Materials*, 2019, **31**, 7864–7876.

[57] J. Chen, W. Deng, X. Gao, S. Yin, L. Yang, H. Liu, G. Zou, H. Hou and X. Ji, *ACS Nano*, 2021, **15**, 6061–6104.

[58] I. I. Abate, C. D. Pemmaraju, S. Y. Kim, K. H. Hsu, S. Sainio, B. Moritz, J. Vinson, M. F. Toney, W. Yang, W. E. Gent, T. P. Devereaux, L. F. Nazar and W. C. Chueh, *Energy & Environmental Science*, 2021.

[59] H. Chen and M. S. Islam, *Chemistry of Materials*, 2016, **28**, 6656–6663.

[60] A. Grenier, G. E. Kamm, Y. Li, H. Chung, Y. S. Meng and K. W. Chapman, *Journal of the American Chemical Society*, 2021, **143**, 5763–5770.

[61] P. Yan, J. Zheng, Z.-K. Tang, A. Devaraj, G. Chen, K. Amine, J.-G. Zhang, L.-M. Liu and C. Wang, *Nature Nanotechnology*, 2019, **14**, 602–608.

[62] W. Yin, A. Grimaud, G. Rousse, A. M. Abakumov, A. Senyshyn, L. Zhang, S. Trabesinger, A. Iadecola, D. Foix, D. Giaume and J.-M. Tarascon, *Nature Communications*, 2020, **11**, 1252.

[63] J. Lee, J. K. Papp, R. J. Clément, S. Sallis, D.-H. Kwon, T. Shi, W. Yang, B. D. McCloskey and G. Ceder, *Nature*

Communications, 2017, **8**, 981.

[64] C. Baur, M.-E. Lăcătuşu, M. Fichtner and R. E. Johnsen, *ACS Applied Materials & Interfaces*, 2020, **12**, 27010–27016.

[65] J. Huang, P. Zhong, Y. Ha, D.-H. Kwon, M. J. Crafton, Y. Tian, M. Balasubramanian, B. D. McCloskey, W. Yang and G. Ceder, *Nature Energy*, 2021.

[66] D. A. Kitchaev, J. Vinckeviciute and A. Van der Ven, *Journal of the American Chemical Society*, 2021, **143**, 1908–1916.

[67] P. Zhong, Z. Cai, Y. Zhang, R. Giovine, B. Ouyang, G. Zeng, Y. Chen, R. Clément, Z. Lun and G. Ceder, *Chemistry of Materials*, 2020, **32**, 10728–10736.

[68] X. Zheng, Z. Xu, S. Li, Y. Zhang, J. Zhang, C. Kuai, L. Tao, M. M. Rahman, Y. Zhang, S.-J. Lee, C.-J. Sun, L. Li, W. Hu, D. Nordlund, J. Liu, Y. Liu and F. Lin, *Acta Materialia*, 2021, **212**, 116935.